ACS Photonics

pubs.acs.org/journal/apchd5

Letter

Compact Incoherent Image Differentiation with Nanophotonic Structures

Haiwen Wang, Cheng Guo, Zhexin Zhao, and Shanhui Fan*

Cite This: *ACS Photonics* 2020, 7, 338–343

Read Online

ACCESS | Metrics & More | Article Recommendations

ABSTRACT: There are significant recent interests in using nanophotonic structures to perform differentiation operation on images for edge detection purposes. All previous works using nanophotonic structures, however, can only operate with coherent light. Here we introduce a hybrid optoelectronic approach that enables one to use nanophotonic structures to perform differentiation operation with incoherent light. As a demonstration, we consider a photonic crystal slab structure and show that differentiation operation with incoherent light can be achieved by subtracting the optical transfer function of the structure at two different frequencies. Our method is robust to noise and directly integrable into existing imaging systems and, thus, points to a new avenue for improving image sensors using nanophotonic structures.

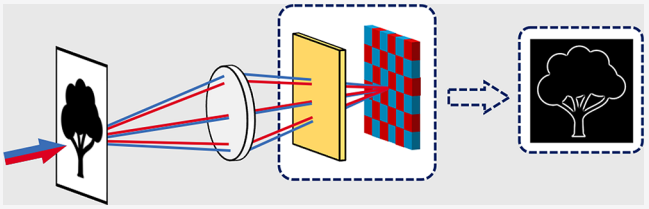

KEYWORDS: *optical image processing, incoherent light, optoelectronic processor, edge detection*

Downloaded via STANFORD UNIV on April 14, 2021 at 01:17:38 (UTC).
See https://pubs.acs.org/sharingguidelines for options on how to legitimately share published articles.

Edge detection is one of the most widely used image processing techniques with many applications.[1−6] It is well-known that edge detection of an incoherent image can be achieved with a Fourier optics setup,[7,8] as shown schematically in Figure 1a. This type of setups create a synthesized point spread function, followed by a signal processing step.[7,9−14] A review of the incoherent image processing in Fourier optics can be found here.[15] These methods involve the use of multiple lenses and are generally bulky (e.g., Figure 1a) or they are not suitable for implementation on modern image sensors. As an alternative, there have been significant recent developments in achieving edge detection instead with the use of nanophotonic structures, including meta-surfaces[16−25] and plasmonic structures,[26,27] as well as structures exhibiting the Brewster effects and the spin Hall effects.[28,29] These structures are far more compact as compared with conventional Fourier optics setup and may be directly integrated into image sensor systems.

All previous works on edge detection using nanophotonic structures assume spatially coherent light. Many practical imaging systems, on the other hand, uses spatially incoherent light. In this Letter, we show that nanophotonic structures, properly designed, can be used for edge detection for spatially incoherent light as well. The results here significantly broaden the capability of nanophotonic structures for image processing applications.

GENERAL PRINCIPLE OF DIFFERENTIATION WITH INCOHERENT LIGHT

We consider an edge detection system for incoherent light based on a photonic crystal slab structure, as illustrated in Figure 1b. Photonic crystal slab structures have been previously used to perform differentiation for coherent light.[17,20,23] The operating mechanism for performing differentiation for incoherent light, however, is completely different, as is known in Fourier optics, and we will briefly review here. We assume the slab has a periodicity that is smaller than the wavelength of light, such that for near-normal incident light there is no diffraction. For illustration purposes, we first consider a hypothetical optical structure that is periodic in-plane and has no diffraction effect for light incident from any angle. (A realistic simulation of a physical photonic crystal slab structure will be provided in the later part of the paper.) For an incident coherent light with an amplitude $E_{in}(k)$, where k is an in-plane wavevector parallel to the slab, we denote the amplitude transmission coefficient as $t(k)$ such that $E_{out}(k) = t(k)E_{in}(k)$. Suppose we consider an incident image that is completely spatially incoherent, which means that the electric field at two different spatial locations are completely uncorrelated with each other, that is:

$$\langle E_{in}(x)E_{in}(x')\rangle \propto I_{in}(x)\delta(x - x') \quad (1)$$

where $I_{in}(x)$ is the intensity of incident light. We define the spatial Fourier transformation of the incident intensity as

Received: October 8, 2019
Published: January 22, 2020

ACS Publications © 2020 American Chemical Society

https://dx.doi.org/10.1021/acsphotonics.9b01465
ACS Photonics 2020, 7, 338–343

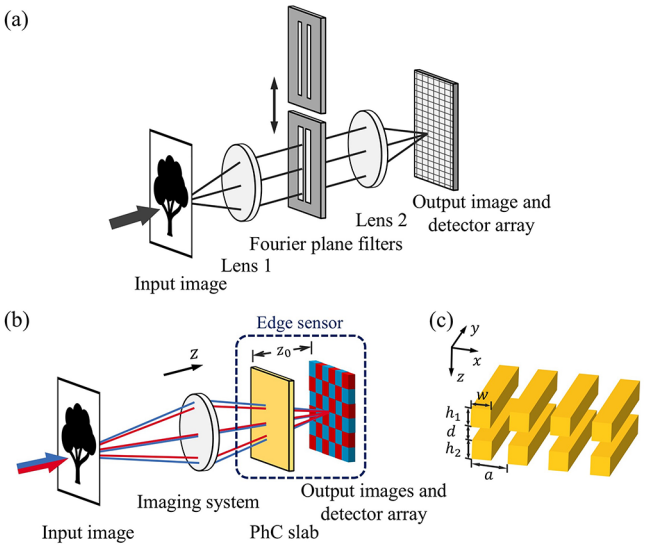

Figure 1. Comparison of the Fourier optics method (a) and our method (b), for spatial differentiation of incoherent images, with our structure shown in (c). In (a), the image is carried by monochromatic light. Either one of the two Fourier plane filters can be used to form image on the detector plane to be subtracted later. In (b), the same image $I_{in}(x)$ is carried by incoherent light at two frequencies, filtered by a photonic crystal slab. The two images of each frequency ($I_{1,out}(x)$, $I_{2,out}(x)$) are collected by detector pixels of corresponding color and subtracted later. The detector pixels are exaggerated for visualization. The structure to achieve incoherent second order differentiation operation is shown in (c). The parameters are $d = 0.57a$, $h_1 = h_2 = 0.55a$, $w = 0.55a$. a is the periodicity along the x direction of the grating. The yellow regions correspond to a material with a refractive index of 2.

$$I_{in}(q) = \int_{-\infty}^{\infty} I_{in}(x)e^{-iqx}\mathrm{d}x \tag{2}$$

Upon passing the incident image through the structure, the output image is described by a spatial intensity distribution $I_{out}(x)$ with its Fourier spectrum:

$$I_{out}(q) = T(q)I_{in}(q) \tag{3}$$

where

$$T(q) = \frac{1}{N}\int_{-\infty}^{\infty} t^*(k)t(k+q)\mathrm{d}k \tag{4}$$

is the Optical Transfer Function (OTF) in Fourier optics[8] and characterizes the incoherent transmission property of the system. Here N is an intensity normalization constant.

From eq 4 it is clear that differentiation cannot be achieved by simply passing an incoherent image $I_{in}(x)$ through an optical structure. Differentiating a uniform field distribution should produce zero. And thus any transfer function that can perform differentiation needs to vanish for the $q = 0$ Fourier component. On the other hand, $|T(q)|$ of eq 4, in fact, maximizes at $q = 0$, as can be proved using the Cauchy–Schwarz inequality. Therefore, in contrast to coherent image processing, for incoherent image no optical structure by itself can perform differentiation.

Spatial differentiation of an incoherent image can be achieved instead with a hybrid optoelectronic approach. In this approach, one passes the input image through two different structures with different optical transfer functions $T_1(q)$ and $T_2(q)$, respectively, to generate two output images $I_{1,out}$ and $I_{2,out}$. For reasons that will be justified below, we assume that near $q = 0$ we have $T_{1,2}(q) = 1 - c_{1,2}q^2$, with $c_1 \neq c_2$. Consider the image $I_{out} \equiv I_{1,out} - I_{2,out}$, as can be obtained by digital computation. From eq 3, we then have $I_{out}(q) = (c_2 - c_1)q^2 I_{in}(q) \equiv T_{eff}(q)I_{in}(q)$. Therefore, $I_{out}(q)$ represents a second-order spatial differentiation of the input image. This is analogous to what was achieved in refs 7 and 9. This method can be easily generalized into 2D image processing, where we can use a two-dimensional photonic crystal slab with $T_{1,2}(q_x,q_y) = 1 - c_{1,2;x}q_x^2 - c_{1,2;y}q_y^2$, and after the same subtraction process, the output is $I_{out}(q_x,q_y) = ((c_{2;x} - c_{1;x})q_x^2 + (c_{2;y} - c_{1;y})q_y^2)I_{in}(q_x,q_y)$.

In Fourier optics, the approach for spatial differentiation of incoherent image, as outlined above, can be achieved by sending an input image through a 4f optical setup consisting of a pair of lens performing forward and reverse Fourier transformation.[7] The required two different optical transfer functions are obtained by placing two different mask structures at the Fourier plane (Figure 1a). This approach requires the use of bulky optics and the involvement of moving parts, hence, is difficult to be integrated into standard imaging systems.

In contrast to the standard Fourier optics approach, here we consider an alternative strategy, shown in Figure 1b. We consider an object illuminated with spatially incoherent light at two different wavelengths. In the absence of the photonic crystal slab, the imaging system generates the same image at two wavelengths onto the detector. For illustration purposes in this paper we assume a one-dimensional image and hence take $k_y = 0$. The key requirement for the photonic crystal slab structure is that it has a large difference in their coherent transmission function $t(k_x)$ at the two frequencies, and therefore the imaging system has different optical transfer functions $T_1(q_x)$ and $T_2(q_x)$ at the two frequencies. By detecting the transmitted images at the two frequencies, and by subtracting the two images by digital computation, we can then obtain a spatial differentiation of the input incoherent light image. We can effectively view the combination of photonic crystal slab and the image sensor, as an edge sensor that is only sensible to edges in spatially incoherent images. This approach requires both optical and electronic processing. Therefore, we refer to this approach as an "optoelectronic" approach.

Unlike the traditional Fourier optics technique as shown in Figure 1a, where the filter structure needs to be placed at the Fourier plane, for our design as shown in Figure 1b, the photonic crystal slab can be placed at any position in front of image plane, and outcome is independent of the position. To see that, we use $t_{img}(k)$ to denote the amplitude transmission for the original imaging system in the absence of the slab, $t_{phc}(k)$ to denote the amplitude transmission of the photonic crystal slab, and $t_{tot}(k)$ to denote the total transmission function of the whole imaging system containing the photonic crystal slab. Assume the photonic crystal slab is placed at z_0 before the image plane. The amplitude transmission at $z = -z_0$ before the photonic crystal slab is therefore $t_{-z_0}(k) = t_{img}(k)e^{-iz_0\lambda k^2/4\pi}$. The total transmission function can thus be calculated to be

$$t_{tot}(k) = t_{-z_0}(k)t_{phc}(k)e^{iz_0\lambda k^2/4\pi} = t_{img}(k)t_{phc}(k) \tag{5}$$

Here, λ is the wavelength of a quasi-monochromatic light. Notice that the total transmission is independent of the position z_0 of the photonic crystal slab. Thus, we can in fact

https://dx.doi.org/10.1021/acsphotonics.9b01465
ACS Photonics 2020, 7, 338−343

directly put the photonic crystal slab directly onto the image sensor, therefore, such an edge sensor can be made compact.

We note that in many standard image detection systems, such as CMOS image sensor arrays, images at multiple color channels are detected simultaneously.[30] Therefore, in practice, one can illuminate an object simultaenously with multiple wavelengths, and also take images at multiple wavelengths at the same time. This method eliminates the need of any moving elements, compared to the standard Fourier optics approach. The photonic crystal slab device can be integrated directly onto the image sensor therefore leaving the design of the imaging system unchanged. The integration eliminates the bulky 4f optical setup and results in a structure that is far more compact and is directly integrable with standard image detection systems.

Differentiation and edge detection can certainly be achieved in the digital domain. Since our approach also requires digital computation, it is of use to compare the computational cost required between our approach and the standard digital approach. In the standard digital approach, the edge detection is achieved by a LoG filter, which uses a convolution kernel results from a Laplacian on a Gaussian (LoG) function.[1] Assuming that the image has $N \times N$ pixel, and the filter size is $a \times a$, the computational cost is approximately $2a^2N^2$, with a^2 typically on the order of 9 or larger. On the other hand, in our approach, the digital computation required include a summation over all pixels for normalization, followed by a point-by-point subtraction. The total computational cost is approximately $4N^2$. Thus, the computational cost in our approach is significantly lower. Reducing the computational cost for edge detection is important in particular in mobile and edge computing devices where the computational power available at the device is limited.

SECOND ORDER DIFFERENTIATION ON AN INCOHERENT IMAGE

Based on the discussions above, we designed a photonic crystal slab structure, shown in Figure 1c, to perform second order differentiation on 1D incoherent image. The structure has two layers of dielectric rods which are infinite along y-axis but periodically spaced with period a along the x-axis. We consider image projected onto the slab along the z-direction, with an electric field polarization along the y-axis. The optical transfer function $T(q_x)$, of an optical structure in general satisfies:

$$T(-q_x) = T^*(q_x) \tag{6}$$

as can be seen from the definition of the autocorrelation function. Moreover, in our structure, the $x = 0$ plane is a mirror symmetry plane. Thus, from the mirror symmetry, the amplitude transmission function has the property:

$$t(k_x) = t(-k_x) \tag{7}$$

Using this relation, we get:

$$T(q_x) = T(-q_x) \tag{8}$$

Therefore, combined with eq 6, we see that $T(q_x)$ is a real and even function. We thus have $T(q_x) = 1 - cq_x^2$ around $q_x = 0$, where $T(q_x = 0) = 1$ is set by normalization. Subtraction of two different OTFs gives a quadratic function in q_x and leads to a second order differentiation.

To illustrate this concept, the transmission of a two-layer photonic crystal slab structure (Figure 1c) is calculated for different frequencies and wavevectors[31] and shown in Figure 2a. The regions in the frequency−wavevector space with high

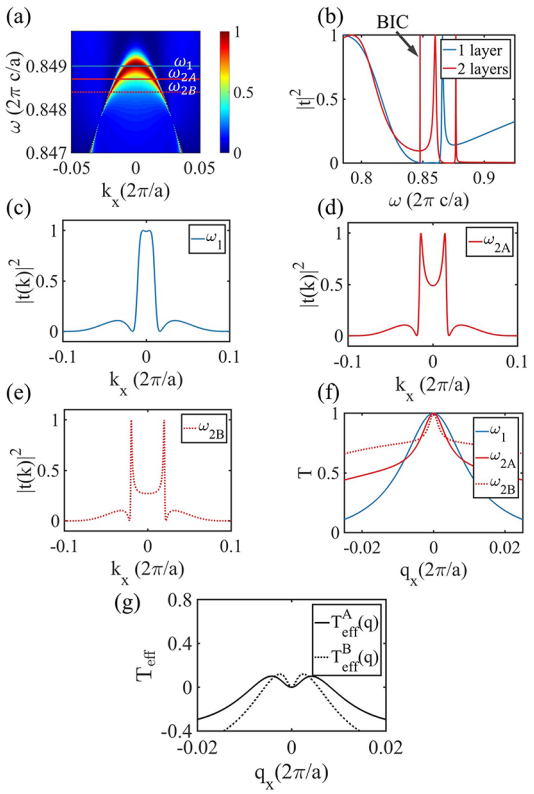

Figure 2. Realization of second order differentiation on incoherent input image. (a) Intensity transmission for coherent light, at different frequency ω and in-plane wavevector k_x. (b) Intensity transmission versus frequency for incident light with $k_x = 0.028 \times 2\pi c/a$, for single layer of grating and two-layer grating structures. (c−e) Intensity transmission for coherent light as a function of wavector k_x at frequencies $\omega_1 = 0.8490 \times 2\pi c/a$, $\omega_{2A} = 0.8487 \times 2\pi c/a$ and $\omega_{2B} = 0.8484 \times 2\pi c/a$, respectively. (f) Optical transfer function for incoherent light as a function of wavevector q_x, as calculated from (c), (d), and (e). (g) Effective intensity transmission function for incoherent light, as obtained from the subtraction of two curves in (f).

transmission correspond to the resonances of the structure. We note the existence of a bound state in continuum at $k_x = \pm 0.028 \times 2\pi/a$, and $\omega = 0.8478 \times 2\pi c/a$, where the resonance linewidth vanishes. The existence of such a bound state in continuum can be understood by analyzing the transmission of a single layer at $k_x = 0.028 \times 2\pi/a$, as shown in Figure 2b. The reflection of a single layer reaches 100% at the frequency $\omega = 0.851 \times 2\pi c/a$ due to the guided resonance effect.[32] By choosing the thickness of the air layer between the slab to be $d = 0.57a$, a Fabry−Perot resonance of the two-layer structure is located at a nearby frequency $\omega = 0.8478 \times 2\pi c/a$, due to the shifting of resonance by interlayer coupling.[33] Such a Fabry−Perot resonance has a zero linewidth and forms a bound state in continuum (BIC).[34,35] In the vicinity of the BIC, the transmission spectrum of the two-layer structure shows a strong frequency dependency, as seen by comparing Figure 2c, d, and e, which show the transmission spectra at frequencies $\omega_1 = 0.8490 \times 2\pi c/a$,$\omega_{2A} = 0.8487 \times 2\pi c/a$, and $\omega_{2B} = 0.8484 \times 2\pi c/a$, respectively.

Starting from the coherent transmission function, we now compute the OTF, shown in Figure 2f. Here, instead of

https://dx.doi.org/10.1021/acsphotonics.9b01465
ACS Photonics 2020, 7, 338−343

assuming the correlation function of eq 1, which has a vanishing correlation length, we use a more realistic form of correlation function:

$$\left\langle E_{\text{in}}^{*}\left(x-\frac{\delta x}{2}\right)E_{\text{in}}\left(x+\frac{\delta x}{2}\right)\right\rangle = I_{\text{in}}(x)\frac{1}{\Delta}\exp\left(-\frac{\delta x^{2}}{4\Delta^{2}}\right) \tag{9}$$

where Δ is the transverse correlation length, which is assumed to be small compared to the image size. In the spatial frequency domain, the correlation becomes

$$\langle E_{\text{in}}^{*}(k_x')E_{\text{in}}(k_x)\rangle \propto I(k_x-k_x')\exp\left(-\frac{\Delta^{2}(k_x'+k_x)^{2}}{4}\right) \tag{10}$$

We can then calculate the output intensity (with $q_x = k_x - k_x'$):

$$I_{\text{out}}(x) = \langle E_{\text{out}}^{*}(x)E_{\text{out}}(x)\rangle \tag{11}$$

$$\propto\int_{-\infty}^{\infty}I(q_x)\int_{-\infty}^{\infty}t^{*}(k_x')t(k_x'+q_x)\exp\left(-\frac{\Delta^{2}(2k_x'+q_x)^{2}}{4}\right)\mathrm{d}k_x'\exp(iq_xx)\mathrm{d}q_x \tag{12}$$

The OTF shown in Figure 2f is therefore the following quantity:

$$T(q_x) = \frac{1}{N}\int_{-\infty}^{\infty}t^{*}(k_x)t(k_x+q_x)\exp\left(-\frac{\Delta^{2}(q_x+2k_x)^{2}}{4}\right)\mathrm{d}k_x \tag{13}$$

We assume that the incoherent image significantly varies only at a length scale much larger than the wavelength; hence, the relevant q_x is small. The exponential factor in eq 13 then ensures that for $t(k_x)$ only those components with small k_x contribute to $T(q_x)$. In the numerical calculation, we choose $\Delta = 25a/2\pi$ and choose the normalization factor N, such that $T(q = 0) = 1$. This transverse correlation length Δ corresponds to 3.4λ. According to the van Cittert-Zernike theorem, this transverse correlation length approximately correspond to that of an incoherent image formed by an optical system having a lens with its numerical aperture characterized by an F-number of 12.[36] At the operating frequency, propagating light within the numerical aperture of such an optical system, when passing through the photonic crystal slab, does not experience any diffraction effect. The OTFs, thus calculated at the three frequencies corresponds to Figure 2c–e, are shown in Figure 2f. These OTFs all peak at $q = 0$, a feature that we previously derived analytically assuming the correlation function of eq 1 with a vanishing correlation length. The introduction of a small nonzero correlation length does not change this feature.

In Figure 2g we plot $T_{\text{eff}}^{A}(q_x) = T_{\omega 1}(q_x) - T_{\omega 2A}(q_x)$ and $T_{\text{eff}}^{B}(q_x) = T_{\omega 1}(q_x) - T_{\omega 2B}(q_x)$. The plotted function is an effective intensity transfer function of the system after digital subtraction, we see that they are both quadratic around $q_x = 0$. Therefore, in spatial domain, either one can be used to perform a second order differentiation on the input incoherent image. Figure 3a shows an example image and its exact second order differentiation. Figure 3b shows the corresponding output filtered through T_{eff}^{A} (output A) and T_{eff}^{B} (output B). With either effective intensity transfer function, the output coincides with the second order differentiation operating on the input image.

The two effective intensity transfer function has different curvature at $q_x = 0$. This curvature is determined by the linewidth along k_x in the coherent transmission function. In determining T_{eff}^{A} and T_{eff}^{B}, the coherent transmission function at ω_1 is used in both cases, and the coherent transmission function at ω_{2B} has a smaller linewidth compared to ω_{2A}. Therefore, the OTF for ω_{2B} has a sharper peak at $q_x = 0$ than ω_{2A}, and therefore, $T_{\text{eff}}^{B}(q_x)$ has a larger curvature at $q_x = 0$ than $T_{\text{eff}}^{A}(q_x)$.

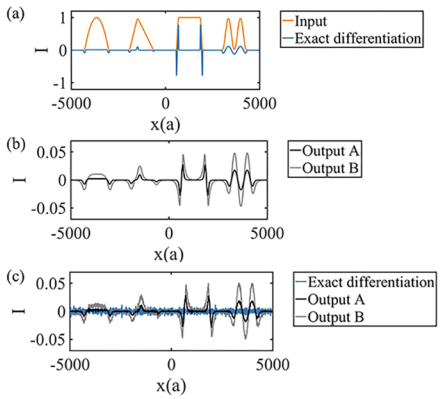

Figure 3. Input and output of the second order differentiator. (a) The input 1D image and exact differentiation of the input. The edges in the input are smoothed for better visualization. (b) Output images of the system, which are filtered by T_{eff}^{A} and T_{eff}^{B}, respectively. (c) Exact differentiation and outputs in the presence of noise on the input image.

Different effective intensity transfer functions generate different output images. A larger curvature of T_{eff} at $q = 0$ generates a larger output signal, shown in Figure 3b by comparing the outputs from T_{eff}^{A} and T_{eff}^{B}. The output B has a larger signal amplitude as compared to output A. This can be understood since for a perfect second order differentiation, where $T_{\text{eff}} = \frac{1}{2}cq_x^{2}$, the output intensity is directly proportional to the curvature c. Another feature that controls the output image is the range of q_x, where T_{eff} remains quadratic. Ideally, we want such range to be as large as possible, so that an accurate differentiation operation can be achieved for sharper image variations. Comparing Figure 3a and b, we see the output A matches closer to the exact second-order differentiation as compared to output B, since T_{eff}^{A} is closer to a quadratic function over a larger range as compared with T_{eff}^{B}. We also tested the spatial resolution of such device using a series of slits with variable width, following the previous paper.[27] The resolutions are around $250a$ for both cases, with the resolution of output A slightly larger. This is another manifestation of the quadratic range of output A being larger.

The subtraction process as used above for generating differentiation usually results in a decreased signal-noise ratio (SNR) in the output compared to the input images. To investigate the effect of noise, we added a band limited ($-0.05 \times 2\pi/a < q < 0.05 \times 2\pi/a$) white noise at the input. The intensity fluctuation is at about 1% of the maximum intensity. In Figure 3c, the differentiation signal using our proposed device is simulated. We clearly see detection of the edges in spite of the presence of noises, for both filters in Figure 2g. Ordinary CMOS image sensors, usually have a dynamic range over 60 dB.[30,37] Thus, the output signal should be readily detectable with standard CMOS image sensor. In comparison, the edges are not clearly visible with an exact numerical differentiation. (Figure 3c, blue line). In digital image processing, edge detection is typically carried out with the use of LoG filter, which possess a convolution kernel with a

https://dx.doi.org/10.1021/acsphotonics.9b01465
ACS Photonics 2020, 7, 338–343

size beyond the nearest neighbor pixel, in order to reduce the noise effects. Our design here produces a similar effect and, hence, is similarly robust against noise in the input image.

FIRST-ORDER DIFFERENTIATION ON AN INCOHERENT IMAGE

In addition to second-order differentation, as discussed above, we see that first-order differentiation of incoherent image is also possible with this method. To achieve this, we use the structure shown in Figure 4a, where the mirror symmetry

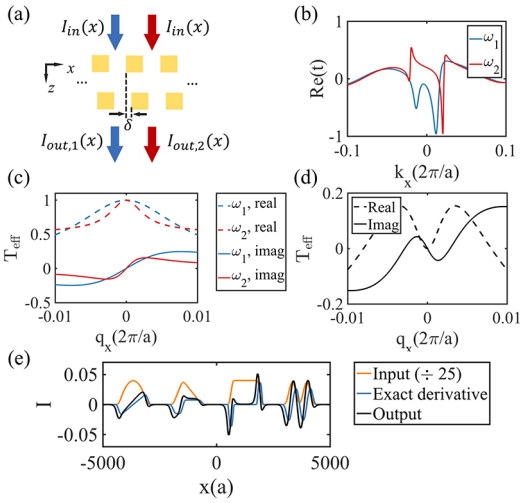

Figure 4. Realization of first order differentiation on incoherent input image. (a) The structure is the same as Figure 1c, except that the second layer is shifted by $\delta = 0.1a$. (b) Numerically calculated coherent amplitude transmission (real part) at two frequencies ω_1 and ω_2. (c) OTF at these two frequencies calculated from (b). (d) Effective intensity transfer function for incoherent light after digital subtraction. (e) Input image, exact first-order derivative of the input, and the output of the system. The edges in the input are smoothed for better visualization.

about $x = 0$ is broken since the second layer is shifted by a distance δ along x. The coherent transmission function is numerically calculated[31] at two frequencies $\omega_1 = 0.8490 \times 2\pi c/a$ and $\omega_2 = 0.8486 \times 2\pi c/a$ (shown in Figure 4b). We see that their real parts are no longer symmetric with respect to $k_x = 0$. The OTFs, calculated using eq 13 at two frequencies, are shown in Figure 4c. In this case, the OTF is no longer real, and its imaginary part must be odd with respect to $q_x = 0$ (see eq 6). Thus, for the lowest order in q_x, the OTF takes the form $T(q_x) = 1 - i\beta q_x$. By subtracting the two OTFs at the two frequencies above, we obtain an effective internsity transfer function that has a linear dependency on q_x around $q_x = 0$ (Figure 4d). This correspond to a first order differentiation in the spatial domain for incoherent image. As an illustration, we show the input image which is the same as in Figure 3a, along with the output image after digital subtraction, in Figure 4e. Over most of the spatial regions, the output corresponds well with a first order differentiation operating on the input image. Moreover, we see some additional peaks at the edges of the input image. This corresponds to a weak second order signal and are caused by the quadratic dependency of $\mathrm{Re}(T_{\mathrm{eff}})$ seen in Figure 4d. The resolution of first order differentiation is similarly tested to be $400a$. In 2D image processing, breaking certain symmetry will similarly lead to first order differentiation.

CONCLUSION

To summarize, we show that by using a hybrid optoelectronic approach, we can achieve incoherent image differentiation with compact nanophotonic structure. Our approach eliminates the use of bulky 4f system and moving parts in conventional Fourier optics methods, and achieves image differentiation using compact and planar structure with wavelength scale thickness. While here for illustration purposes we assume that the input light has two frequencies and, hence, has a high degree of temporal coherence, the result can be generalized to incident light with broader bandwidth. The quality factors of the resonances that we use in the paper are on the order of 10^3. Experimentally, guided resonance with quality factor exceeding 10^5 has been demonstrated.[38] Thus, our structure should be amenable to current nanofabrication capabilities. Our device is robust to input noise compared to exact differentiation. The photonic crystal slab filter, being a spatial frequency domain filter, can be directly integrated onto existing CMOS image sensors. Our proposed method points to a new avenue of using nanophotonic structures to improve imaging sensors with potential applications in real scene image processing and object recognition.

AUTHOR INFORMATION

Corresponding Author

Shanhui Fan − *Department of Electrical Engineering and Ginzton Laboratory, Stanford University, Stanford, California 94305, United States*; Email: shanhui@stanford.edu

Authors

Haiwen Wang − *Department of Applied Physics and Ginzton Laboratory, Stanford University, Stanford, California 94305, United States*; orcid.org/0000-0001-7414-0776

Cheng Guo − *Department of Applied Physics and Ginzton Laboratory, Stanford University, Stanford, California 94305, United States*

Zhexin Zhao − *Department of Electrical Engineering and Ginzton Laboratory, Stanford University, Stanford, California 94305, United States*

Complete contact information is available at: https://pubs.acs.org/10.1021/acsphotonics.9b01465

Notes

The authors declare no competing financial interest.

ACKNOWLEDGMENTS

The work is supported by Samsung electronics and by a AFOSR MURI Project (FA9550-17-1-0002). The authors thank Prof. Meir Orenstein and Dr. Avik Dutt for helpful discussions.

REFERENCES

(1) Gonzalez, R. C.; Woods, R. E. *Digital Image Processing*; Pearson Higher Ed, 2011.

(2) Shrivakshan, G. T.; Chandrasekar, C. A comparison of various edge detection techniques used in image processing. *International Journal of Computer Science Issues* **2012**, *9*, 269−276.

(3) Roddier, F. Curvature sensing and compensation: a new concept in adaptive optics. *Appl. Opt.* **1988**, *27*, 1223−1225.

(4) Marmanis, D.; Schindler, K.; Wegner, J. D.; Galliani, S.; Datcu, M.; Stilla, U. Classification with an edge: Improving semantic image segmentation with boundary detection. *ISPRS Journal of Photogrammetry and Remote Sensing* **2018**, *135*, 158−172.

(5) Chen, L.-C.; Barron, J. T.; Papandreou, G.; Murphy, K.; Yuille, A. L. Semantic Image Segmentation with Task-Specific Edge Detection Using CNNs and a Discriminatively Trained Domain Transform. *IEEE Conference on Computer Vision and Pattern Recognition* **2016**, 4545−4554.
(6) Choudhry, P. High-Throughput Method for Automated Colony and Cell Counting by Digital Image Analysis Based on Edge Detection. *PLoS One* **2016**, *11*, No. e0148469.
(7) Gorlitz, D.; Lanzl, F. Methods of zero-order non-coherent filtering. *Opt. Commun.* **1977**, *20*, 68−72.
(8) Goodman, J. W. *Introduction to Fourier optics*; Roberts and Company Publishers, 2005.
(9) Kelly, D. H. Image-processing experiments. *J. Opt. Soc. Am.* **1961**, *51*, 1095−1101.
(10) Stoner, W. Edge enhancement with incoherent optics. *Appl. Opt.* **1977**, *16*, 1451−1453.
(11) Rhodes, W. T. Bipolar pointspread function synthesis by phase switching. *Appl. Opt.* **1977**, *16*, 265−267.
(12) Leith, E. N.; Angell, D. K. Generalization of some incoherent spatial filtering techniques. *Appl. Opt.* **1986**, *25*, 499−502.
(13) Lohmann, A. W. Incoherent optical processing of complex data. *Appl. Opt.* **1977**, *16*, 261−263.
(14) Angell, D. K. Incoherent spatial filtering with grating interferometers. *Appl. Opt.* **1985**, *24*, 2903−2906.
(15) Rhodes, W. T. Incoherent Spatial Filtering. *Opt. Eng.* **1980**, *19*, 323−330.
(16) Silva, A.; Monticone, F.; Castaldi, G.; Galdi, V.; Alu, A.; Engheta, N. Performing Mathematical Operations with Metamaterials. *Science* **2014**, *343*, 160−163.
(17) Guo, C.; Xiao, M.; Minkov, M.; Shi, Y.; Fan, S. Photonic crystal slab Laplace operator for image differentiation. *Optica* **2018**, *5*, 251−256.
(18) Kwon, H.; Sounas, D.; Cordaro, A.; Polman, A.; Alù, A. Nonlocal Metasurfaces for Optical Signal Processing. *Phys. Rev. Lett.* **2018**, *121*, 173004.
(19) Bykov, D. A.; Doskolovich, L. L.; Bezus, E. A.; Soifer, V. A. Optical computation of the Laplace operator using phase-shifted Bragg grating. *Opt. Express* **2014**, *22*, 25084−25092.
(20) Golovastikov, N. V.; Bykov, D. A.; Doskolovich, L. L. Resonant diffraction gratings for spatial differentiation of optical beams. *Quantum Electron.* **2014**, *44*, 984−988.
(21) Pors, A.; Nielsen, M. G.; Bozhevolnyi, S. I. Analog Computing Using Reflective Plasmonic Metasurfaces. *Nano Lett.* **2015**, *15*, 791−797.
(22) Guo, C.; Xiao, M.; Minkov, M.; Shi, Y.; Fan, S. Isotropic wavevector domain image filters by a photonic crystal slab device. *J. Opt. Soc. Am. A* **2018**, *35*, 1685−1691.
(23) Fang, Y.; Ruan, Z. Optical spatial differentiator for a synthetic three-dimensional optical field. *Opt. Lett.* **2018**, *43*, 5893−5896.
(24) Davis, T. J.; Eftekhari, F.; Gómez, D. E.; Roberts, A. Metasurfaces with Asymmetric Optical Transfer Functions for Optical Signal Processing. *Phys. Rev. Lett.* **2019**, *123*, 013901.
(25) Zhou, J.; Qian, H.; Chen, C.-F.; Zhao, J.; Li, G.; Wu, Q.; Luo, H.; Wen, S.; Liu, Z. Optical edge detection based on high-efficiency dielectric metasurface. *Proc. Natl. Acad. Sci. U. S. A.* **2019**, *116*, 11137−11140.
(26) Ruan, Z. Spatial mode control of surface plasmon polariton excitation with gain medium: from spatial differentiator to integrator. *Opt. Lett.* **2015**, *40*, 601−4.
(27) Zhu, T.; Zhou, Y.; Lou, Y.; Ye, H.; Qiu, M.; Ruan, Z.; Fan, S. Plasmonic computing of spatial differentiation. *Nat. Commun.* **2017**, *8*, 1−6.
(28) Youssefi, A.; Zangeneh-Nejad, F.; Abdollahramezani, S.; Khavasi, A. Analog computing by Brewster effect. *Opt. Lett.* **2016**, *41*, 3467−3470.
(29) Zhu, T.; Lou, Y.; Zhou, Y.; Zhang, J.; Huang, J.; Li, Y.; Luo, H.; Wen, S.; Zhu, S.; Gong, Q.; Qiu, M.; Ruan, Z. Generalized Spatial Differentiation from the Spin Hall Effect of Light and Its Application in Image Processing of Edge Detection. *Phys. Rev. Appl.* **2019**, *11*, 1.
(30) Nakamura, J. *Image sensors and signal processing for digital still cameras*; CRC Press, 2016.
(31) Liu, V.; Fan, S. S4: A free electromagnetic solver for layered periodic structures. *Comput. Phys. Commun.* **2012**, *183*, 2233−2244.
(32) Fan, S.; Joannopoulos, J. D. Analysis of guided resonances in photonic crystal slabs. *Phys. Rev. B: Condens. Matter Mater. Phys.* **2002**, *65*, 3294−3298.
(33) Marinica, D. C.; Borisov, A. G.; Shabanov, S. V. Bound States in the Continuum in Photonics. *Phys. Rev. Lett.* **2008**, *100*, 183902.
(34) Suh, W.; Yanik, M. F.; Solgaard, O.; Fan, S. Displacement-sensitive photonic crystal structures based on guided resonance in photonic crystal slabs. *Appl. Phys. Lett.* **2003**, *82*, 1999−2001.
(35) Hsu, C. W.; Zhen, B.; Stone, A. D.; Joannopoulos, J. D.; Soljačić, M. Bound states in the continuum. *Nature Reviews Materials* **2016**, *1*, 16048.
(36) Born, M.; Wolf, E. *Principles of Optics: Electromagnetic Theory of Propagation, Interference and Diffraction of Light*; Elsevier, 2013.
(37) Bigas, M.; Cabruja, E.; Forest, J.; Salvi, J. Review of CMOS image sensors. *Microelectron. J.* **2006**, *37*, 433−451.
(38) Hsu, C. W.; Zhen, B.; Lee, J.; Chua, S.-L.; Johnson, S. G.; Joannopoulos, J. D.; Soljačić, M. Observation of trapped light within the radiation continuum. *Nature* **2013**, *499*, 188−191.

https://dx.doi.org/10.1021/acsphotonics.9b01465
ACS Photonics 2020, 7, 338−343